Microfluidic Immunoarray for Point-of-Care Detection of Cytokines in COVID-19 Patients

Ketki S. Bhalerao,[⊥] P. I. Thilini De Silva,[⊥] Keshani Hiniduma,[⊥] Ami Grunbaum, Nicholas Rozza, Richard Kremer, and James F. Rusling*

Read Online

ACCESS | Metrics & More | Article Recommendations | Supporting Information

ABSTRACT: The "cytokine storm" often induced in COVID-19 patients contributes to the onset of "acute respiratory distress syndrome" (ARDS) accompanied by lung infection and damage, multiorgan failure, and even death. This large increase in pro-inflammatory cytokines in blood may be related to severity. Rapid, on-demand cytokine analyses can thus be critical to inform treatment plans and improve survival rates. Here, we report a sensitive, low-cost, semiautomated 3D-printed microfluidic immunoarray to detect 2 cytokines and CRP simultaneously in a single 10 μL serum sample in 25 min. Accuracy was validated by analyzing 80 COVID-19 patient serum samples, with results well correlated to a commercial Meso Scale protein immunoassay. Capture antibodies immobilized in detection microwells in a flat well plate-type flow chamber facilitate the immunoassay, with a programmable syringe pump automatically delivering reagents. Chemiluminescence signals were captured in a dark box with a CCD camera integrated for 30 s. This system was optimized to detect inflammation biomarkers IL-6, IFN-γ, and CRP simultaneously in blood serum. Ultralow limits of detection (LODs) of 0.79 fg/mL for IL-6, 4.2 fg/mL for CRP, and 2.7 fg/mL for IFN-γ with dynamic ranges of up to 100 pg/mL were achieved. ROC statistical analyses showed a relatively good diagnostic value related to the samples assigned WHO COVID-19 scores for disease severity, with the best results for IL-6 and CRP. Monitoring these biomarkers for coronavirus severity may allow prediction of disease severity as a basis for critical treatment decisions and better survival rates.

INTRODUCTION

The COVID-19 pandemic caused by the acute respiratory syndrome coronavirus 2 (SARS-CoV-2) has had an unprecedented impact on the world's health, economy, and societal issues[1,2] and has claimed nearly 8 million lives worldwide since late 2019.[3] The typical route of infection is via aerosolized viral particle uptake by the respiratory tract.[4] While disease manifestation is often mild, it can often become severe and even fatal within hours. An intricate interplay between the virus and the human immune system underlies this complexity. RT-PCR is the gold standard for detecting the virus, but the result is reported qualitatively as either positive or negative.[5−7] Available qRT-PCR tests have the ability to quantify results with great accuracy; however, the tests are time-consuming and expensive, requiring expertise that makes them unsuitable for point-of-care testing. Other tests available to detect COVID-19 include serological and molecular tests that detect antibodies and antigens in COVID-19[8] and lack sensitivity for early detection where the concentrations are low.[8] While nasopharyngeal viral load has been shown to correlate with cytokine levels,[9] neither RT-PCR nor other existing coronavirus tests have proven to be useful measures of existing or predictors of ultimate infection severity.

There is a clear need for tests for COVID-19 and future coronavirus pandemics that can predict disease severity among infected individuals, as well as monitor the cellular basis of virus-induced immune response.[10−12] Efforts have been made to identify biomarkers, prognostic tools, and therapeutic options by studying the cellular basis of immune responses to SARS-CoV-2,[13] and specific panels of cytokines have emerged as critical biomarkers of COVID-19 progression and severity.[14−16] However, the turnaround time of current methodologies of single patient cytokine measurements is too long for the timely workup necessary to guide rapid clinical treatment.
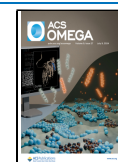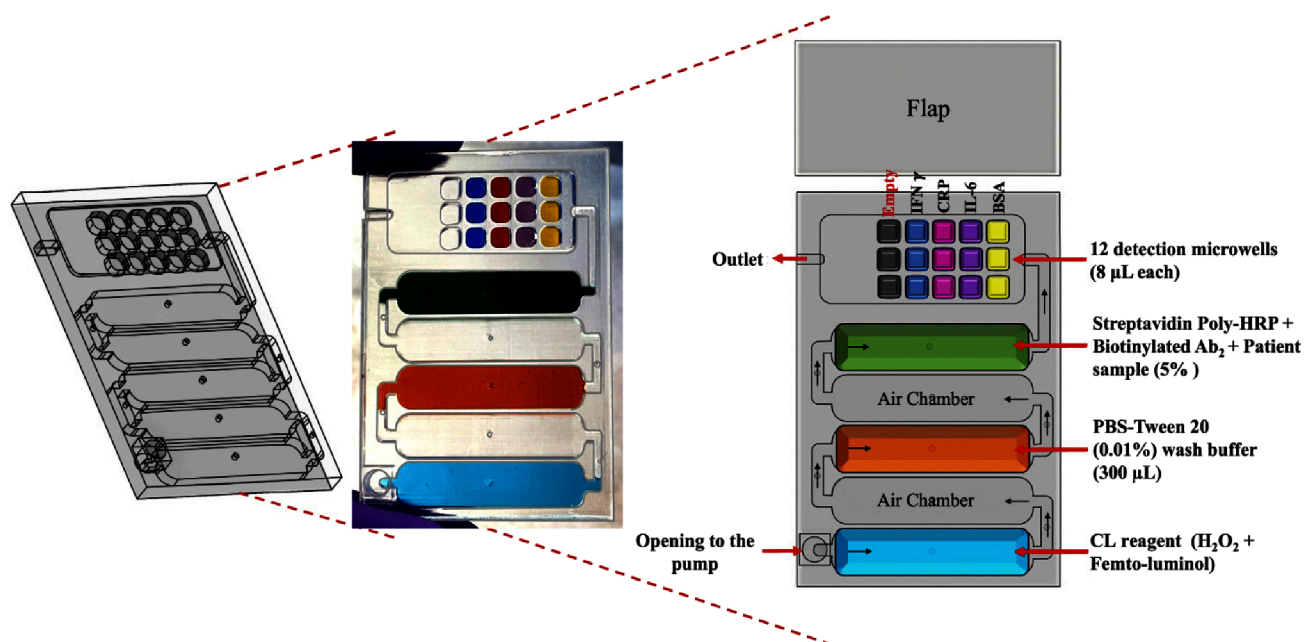
Figure 1. Representations of 3D-printed immunoarray design with unique tray of microwells (3 mm × 3 mm × 1.25 mm each) in the detection chamber.[59] The immunoarray features reagent chambers (larger colored rectangles) to hold a mixture of sample-biotinylated Ab$_2$-ST-PolyHRP, wash buffer, and CL reagent for chemiluminescence detection serially.

Cytokines are small proteins secreted primarily by immune cells that play a critical role in regulating the immune response to infections and are biomarkers for inflammation caused by diseases including cancers.[17] They are molecular messengers that are widely present in body fluids, like blood, saliva, sweat, urine, tears, interstitial fluids (ISFs), and cerebrospinal fluids (CSFs),[39] acting locally and help regulate cell growth, differentiation, and activation,[18−20] which determine cytokine response to disease. In certain cases, an excessive and uncontrolled release of pro-inflammatory cytokines occurs, leading to the hyperactive immune "cytokine storm" or hypercytokinemia.[21,22] This overreaction of the immune system can result in severe tissue damage, serious infections in lungs and kidneys, and possibly death.[23−25] COVID-19 cytokine storm is related to disease severity and clinical outcome.[13,26,27] The resulting acute respiratory distress syndrome (ARDS) causes aggravation and widespread tissue damage that can lead to multiorgan failure and death.[28,29] Consistent with this hypothesis, high levels of proinflammatory cytokines and chemokines including IFN-γ, TNF-α, IL-6, IL-1β, IL-18, CXCL8, CXCL10,[30] and the acute inflammatory protein CRP[24−38] have been found in patients who died from COVID-19.[14,39] Difficulties have been identified in predicting the severity of COVID-19 from tests that measure viral load such as RT-PCR.[40−42] Serological tests can find antibodies against SARS-CoV-2 due to recent or past COVID-19 infections or vaccinations and are not directly related to severity.[43] Current methods for quantifying cytokines in the clinic include immunoassays such as traditional enzyme-linked immunosorbent assay (ELISA) and enzyme-linked immunosorbent spot (ELISpot) and bioassays such as Luminex bead-based assays, flow cytometry assays, and the Meso Scale MSD-ECL assays used as referee assays in this paper. Although these approaches show tremendous promise, they are expensive, have relatively high LODs in the 1−10 pg/mL range for most proteins, and are designed for multiple sample runs.[44−47,50] This makes them unsuitable for single patient POC use. More

recent technology includes single protein counting immunoassays[48,49] for protein detection like the Quanterix Simoa HD-1/X Analyzer.[47,50] These are characterized by excellent LODs in the 2−50 fg/mL range and low reagent and sample volumes. However, single protein counting approaches have high instrument and per-assay costs and are unsuitable for individual patient POC diagnostics. In the early days of the COVID-19 infection, there was no way of predicting the course of the infection in terms of severity by doctors treating patients presented with symptoms of COVID-19 and tested positive for the infection. Early detection of biomarker cytokines with high sensitivity and specificity is a possible approach to predicting disease severity in confirmed COVID-19 patients and could lead to better treatment plans and improve survival rates.[51−53] In this context, a point-of-care (POC) cytokine test readily accessible to physicians in acute settings such as emergency rooms and intensive care units or in resource-limited locations would be of great value.

The World Health Organization (WHO) defined a severity index for COVID-19 based on physician's assessments of symptoms and routine tests.[54,55] Asymptomatic individuals and those with limited symptoms are categorized by WHO scores of 1−2. Moderately symptomatic individuals who require no or need little supplemental oxygen are categorized with WHO scores of 3−4. Patients who show extreme symptoms and have a requirement for supplemental high-flow oxygen, mechanical ventilation, and multiorgan support are classed as "severe" and assigned WHO scores 5−8.[56−58]

Herein, we describe a fast, low-cost, highly sensitive point-of-care immunoassay to detect 3 proinflammatory biomarkers that play a significant role in the cytokine storm in a single assay and provide test results in approximately 25 min. The assay was developed and optimized using our recently designed general 3D-printed immunoarray platform[59] for single sample analyses to enable fast POC measurements for individual COVID-19 patients. The new ultrasensitive assay determines blood serum levels of cytokines IL-6, IFN-γ, and CRP with
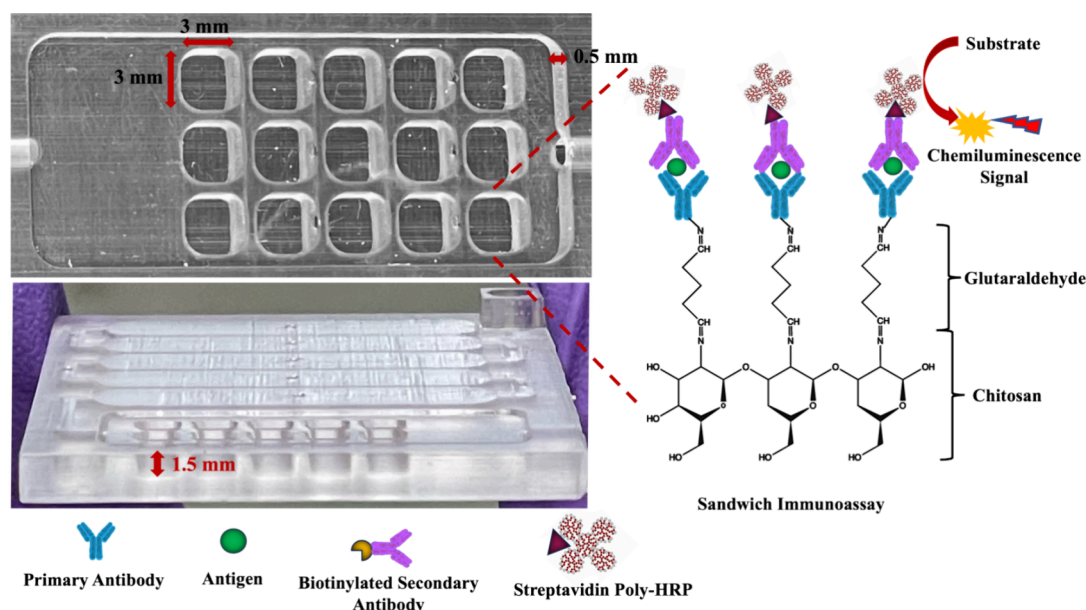
Figure 2. Photographs of the unique microwells in the detection chamber of the 3D-printed immunoarray showing top and side (on bottom) views. Each microwell is 3 mm × 3 mm × 1.25 mm in dimension, with a volume capacity of 8−10 μL. The procedure performs a separate sandwich immunoassay in each of the wells.

limits of detection (LODs) in the low fg/mL range. Our array designed for single, low-cost sample POC assays has much lower LODs than most commercial protein immunoassays that are expensive and designed to analyze relatively large numbers of samples simultaneously in a central lab. Except for recently introduced but expensive single protein detection devices,[60] most ELISA-based commercial protein detection methods are limited by LODs above 1 pg/mL. Recently published POC testing approaches[61] include the use of aptamer beacons for IFN-γ only,[62] with LOD ~ 2 ng/mL, while in our patient data set reported here, the lowest values of IFN-γ are 1 pg/mL. Also, single protein biomarker assays are of limited value for reliable disease diagnostics.[63] Other label-free detection methods for cytokines (2 proteins only) offer comparable assay times of 30−35 min[64,65] but with the best LODs for the 0.4 to 0.9 pg/mL range for cytokines such as IL-1β (lowest values in our data set are 0.01 and 0.8 pg/mL) and TNF-α (lowest values are 0.3 pg/mL). Thus, these assays will not be useful for detection of cytokines in normal control samples or in patients with low impact COVID-19. On the other hand, our assay reported in this paper achieves LODs at least 1000-times lower than the above-referenced recently published POC methods for cytokines, as well as existing commercial methods

Additionally, we have, for the first time in this paper, analyzed our multiplexed cytokine assay data to relate concentrations of 3 relevant cytokines to the severity of COVID-19 infections by correlating results with the WHO severity index assigned to the patients. Sensitive analysis of 80 patient serum samples, involving a cohort of low, medium, and high severity, and further statistical analysis of the concentrations established correlations of cytokine levels with the severity of COVID-19. This can be valuable in the management of future coronavirus infections by enabling guidance for timely medication and treatment for patients likely to present the most serious infections.

■ MATERIALS AND METHODS

Reagents and Samples. Sources of chemicals and proteins are detailed in the Supporting Information. Thermo Fisher Supersignal West Femto was the chemiluminescence (CL) substrate in solution form containing femto-luminol and hydrogen peroxide mixed in a 1:1 ratio right before use. CL was measured within the array in a dark box (Syngene G: box F3) using a CCD camera, and images obtained were processed using GeneSnap software. Human COVID-19 patient serum samples were collected at McGill University Health Centre Research Institute (MUHC-RI) with approval (#2021-6081) from the center's Ethics Board.

3D-Printed Microfluidic Device. Immunoarrays (Figure 1) were constructed via Autodesk Fusion 360 CAD software and then transferred to a Formlabs Form 3 stereolithographic 3D printer to print compact, light-transparent arrays using Formlabs SLA photopolymer V4 resin. Freshly printed arrays are cleaned by sonicating and washing with isopropanol for 10−15 min to remove uncured resin, followed by air drying. Unique 3D-printed microarrays with cover flaps to cover a detection chamber in an open "well-plate" arrangement (Figure 2) were thus designed and constructed simultaneously. There are 15 microwells within the detection chamber (3 rows and 5 columns) of each array, having a volume capacity of 8 microL each. After the wells are equipped with antibodies, cover flaps are pasted onto the top of the microwell array using Loctite Flexible Adhesive and sealed using Gorilla Clear Grip glue. A Chemyx Fusion Touch programmable syringe pump was used for fluidics. Each array is designed to have 3 reagent chambers separated by an air chamber to avoid mixing during flow.

Each downward column of 3 microwells is pre-equipped to detect one of the three target analyte cytokines and CRP simultaneously in a single assay. The very first column closest to the inlet of the detection chamber is used for the control and has no capture antibodies. The control sample used is pooled human serum from Sigma (no COVID-19) with

Scheme 1. Schematic Illustration Showing Steps for the Immobilization of Capture Antibodies with Chitosan and Glutaraldehyde on a Transparent 15-Microwell Immunoarray, Followed by the Sandwich Immunoassay in One Step, and Chemiluminescence Detection (CL) Signal Generation Measured in a Dark Box with a CCD Camera
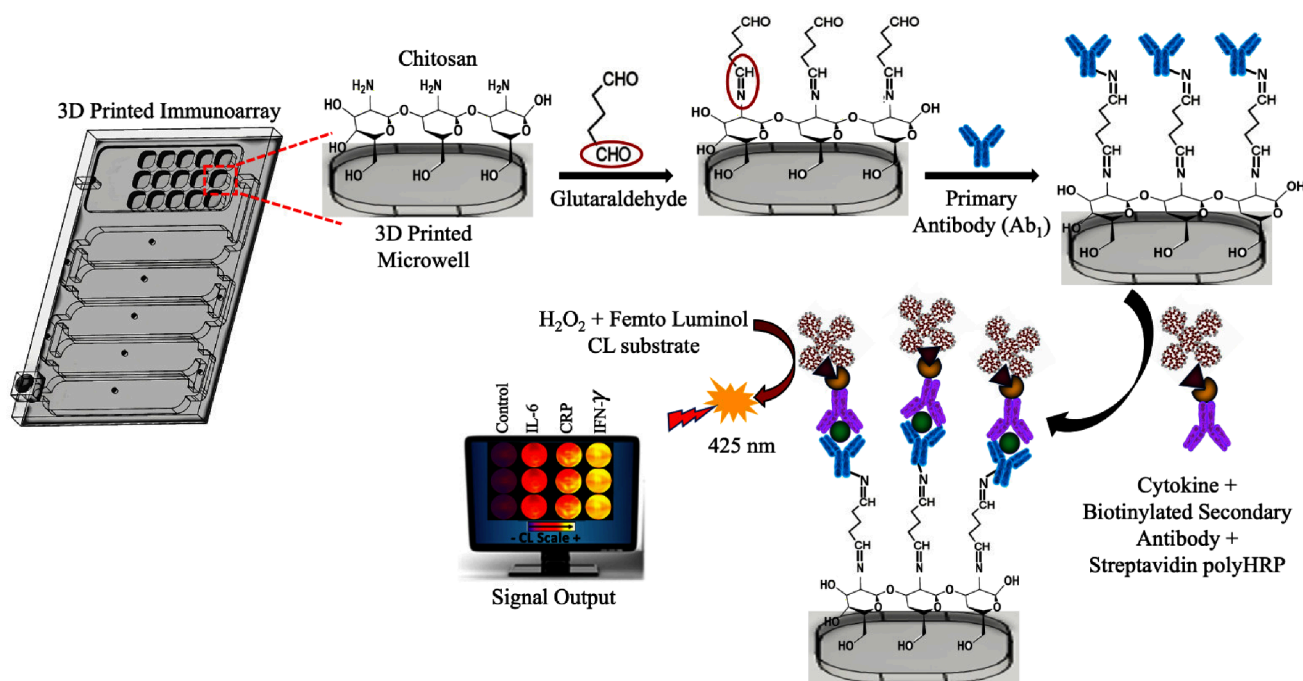
normal levels of cytokines and is representative of the matrix. The control detection column is followed downstream by wells equipped with capture antibodies that bind IL-6, CRP, and IFN-γ. The wells in the last column are used as overflow reservoirs to ensure proper filling of the analytical microwells and to help facilitate proper flow of the sample and reagents across all the wells. The total volume of the detection chamber is 260 μL.

The 5 reagent chambers in the array have volumes of 300 μL each. Three reagents are filled in alternating reagent chambers while leaving chambers in between as air-filled chambers. Optimization of the microwell design, size, and flow rate was done to achieve proper filling of the wells and the efficient emptying of the wells with little to no loss of solutions using methods we reported earlier.[59] Detection wells are pretreated with chitosan, glutaraldehyde, and primary antibodies as described in the following section and stored at 4 °C until use. The matching 3D-printed cover flap is used to seal the open detection chamber before running the assay by gluing it above the wells to the main body of the device.

Immobilization of Primary Antibodies in Sensing Microwells. To load capture antibodies for the assay, microwells in the detection chamber are first filled with 8 μL of 0.5 mg/mL chitosan in a 0.05 M HCl, pH 4, solution followed by incubation at room temperature (RT) for 3 h (Scheme 1). The solution is then removed by tapping, while the array is turned upside down. Arrays are dried overnight in a vacuum to provide a hydrogel layer coating the inside surface of the microwells. Wells are then filled with 3% glutaraldehyde in PBS (pH 7.4) and incubated for 3 h so that amine groups in the chitosan layer form Schiff's bases with glutaraldehyde for subsequent attachment of primary antibodies using methods we developed previously.[66,67] The solution is then drained from the wells by turning the device on its side, tapping, and then drying in vacuum for 1 h. A solution of each specific

primary antibody (Ab$_1$) for IL-6, CRP, or IFN-γ is then added to the assigned wells and allowed to incubate overnight at 4 °C (Scheme 1) for the reaction of free glutaraldehyde with amines on the Ab$_1$'s, the concentrations of which were previously optimized (Supporting Information, Tables S1 and S2, and Figures S1 and S2). We have demonstrated previously that chitosan layers with glutaraldehyde-attached capture antibodies (Ab$_1$) form a highly porous hydrogel that is 98−99% water, presenting a porous medium for efficient convective transport of detection antibody−protein complexes to enter and bind to Ab$_1$ for subsequent CL detection.[59,66,67] The number of Ab$_1$'s immobilized in the microwells was estimated using the bicinchoninic acid (BCA) total protein assay,[68] which gave the numbers of antibodies of 4.0×10^{13} IL-6-Ab$_1$/cm^2, 8.6×10^{13} CRP-Ab$_1$/cm^2, and 9.0×10^{12} IFN-γ-Ab$_1$/cm^2 (Figure S4).

Immunoarrays decorated with capture antibodies (Ab$_1$) and stored at 4 °C are first tap-dried to remove the Ab$_1$ solution present in the microwells and then washed 2× with PBS (pH 7.4) and Tween 20 (0.01%) to remove any loosely bound antibodies.[69] Tween 20 is a non-ionic surfactant used in immunoassays extensively as a wash buffer along with PBS or as a blocking buffer independently.[70] It has been found to effectively reduce nonspecific protein adsorption by washing away the unbound substances from the surface of the array. It additionally prevents the formation of bubbles, allowing for uniform washing steps altogether increasing the selectivity of the assay.[71,72] Blocker Casein buffer (pH 7.4, Thermo Fisher) is then added into each of the microwells and incubated for 1 h to ensure the blocking of any nonspecific sites. The solution is then removed by tapping, and the microwells are once again washed with PBS, pH 7.4. The detection chambers are then sealed by gluing the 3D-printed flap in place to facilitate a smooth, automated flow of fluids without leaks. Reagent chambers are filled with reagents, starting with a mixture of
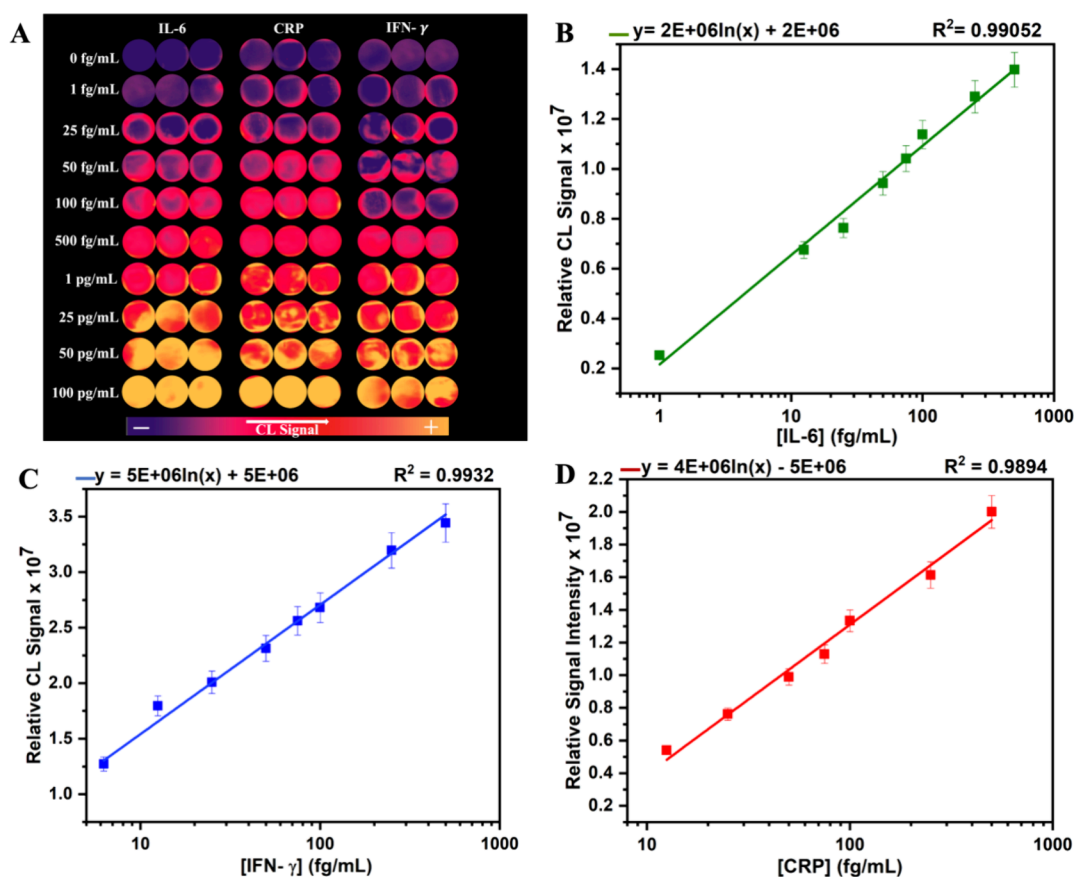
Figure 3. Calibration data for simultaneous detection of cytokines IL-6, CRP, and IFN-γ in buffer-diluted (pH 7.4), 1% pooled human serum with CL captured in a dark box with a CCD camera. (A) Recolorized CL images of 10 immunoarrays showing an increasing CL signal with increasing cytokine concentrations. CL signal response vs concentration for (B) IL-6, (C) CRP, and (D) IFN-γ. Errors bars show standard deviations for $n = 5$.

sample, an optimized concentration 0.5 μg/mL polyHRP-streptavidin conjugate,[44] and biotinylated detection antibodies (Biotin-Ab$_2$) in the top reagent chamber (Figure 1, green), in which streptavidin binds to biotin to form analyte-polyHRP-strepadvadin-Biotin-Ab$_2$ bioconjugates for detection. PBS buffer is placed in the middle reagent chamber (Figure 1, orange) and CL reagent substrate (femto-luminol + H$_2$O$_2$) in the last chamber (Figure 1, blue), leaving alternate second and fourth air chambers empty. Tubing is now connected to a syringe in a programmable syringe pump to control the flow rate at an optimal 150 μL/min (Figure S3). The pump is programmed to flow in steps reflecting the times required to flow reagents to deliver them to the detection chamber and incubate them in the detection chamber for the desired times. In addition, 4 samples can be run simultaneously by the four-syringe pump using different flow lines for 4 immunoarrays. After starting the pump, step 1 flows the analyte-polyHRP-strepadvadin-Biotin-Ab$_2$ bioconjugate into the detection chamber, filling all the microwells. This mixture is incubated in the microwells for 15 min at stopped flow to allow binding of analyte-polyHRP-strepadvadin-Biotin-Ab$_2$ to Ab$_1$ (step 2). Then, the pump restarts, and the solution is pumped out of the wells by the inflow of PBS buffer as a wash to remove excess unbound polyHRP-strepadvadin-Biotin-Ab$_2$. In step 3, the 1:1 femto-luminol-H$_2$O$_2$ mixture flows into the microwells. Once the chamber is filled with this reagent, the flow is stopped, the immunoarray is detached from the pump, and CL images are

captured in the dark box with a CCD camera over a 15 s integration period.

ROC Statistical Analyses. We used receiver-operating characteristic (ROC) analyses of determined cytokine levels grouped by severity derived from physician-assigned WHO severity indices of the patients.[73] ROC plots[74] provide diagnostic utility estimates of sensitivity and specificity, in our case for answering a diagnostic question.[75] We used the assigned independent variables 0, for low disease severity, or independent variable 1, e.g., for the high severity of COVID-19 for each patient sample, to construct x−y ROC plots of true positive rate (sensitivity) vs the false positive rate (100% − specificity) for sample levels as the dependent variables. The closer the curve comes to the upper left corner of the ROC plot, the higher is the diagnostic accuracy. The area under the ROC curve (AUC) is also a measure of diagnostic utility with maximum AUC = 1.0, indicating that dependent variables can perfectly differentiate the independent variables (0 and 1). An ROC curve that lies on the diagonal of the x−y ROC plot axes indicates that the measured variable cannot differentiate between the 0 and 1 states. We used MedCalc ROC software that computes all statistics. The best decision thresholds distinguishing 0 and 1 states are automatically estimated as the value of the dependent variable (e.g., cytokine level), yielding the maximum sum of sensitivity and specificity.

RESULTS

Assay Development. To ensure optimal performance, concentrations of primary capture antibodies (Ab$_1$) and detection antibodies (Ab$_2$) were optimized for the best signal-to-noise ratios and high sensitivity for each cytokine. We optimized concentrations of the specific Ab$_1$ and Ab$_2$ by methods we reported previously[44] (see Tables S1 and S2 and Figures S2 and S3).

The panel of cytokine biomarkers was chosen by considering assays of 57 of the COVID-19 patient serum samples by the Meso Scale Discovery platform by our collaborators at McGill University for cytokines IFN-γ, IL-6, IL1-β, TNF-α, and CRP. Box and whisker plots (Figure S7) and receiver operator curves (ROCs) (Figure S8) were used to find the most promising cytokine biomarkers to differentiate between mild and severe COVID-19 infection based on the WHO severity index, linking the cytokine levels in patient samples to low WHO severity (scores 3 and 4) vs high severity (scores 7 and 8). For the area under the ROC curve (AUC) parameter (Table S4), cytokines giving values closest to 1 were chosen as analytes. IL-6, CRP, and IFN-γ cytokines gave AUC values of 0.789, 0.777, and 0.719, respectively. Thus, we chose these as biomarkers for POC array development and testing.

We established the optimal primary (Ab$_1$) and secondary (Ab$_2$) antibody concentrations, flow rates (Figure S5), and incubation times (Figure S6) to perform calibration measurements for the 3 cytokine standards. The relative CL responses from the 3D-printed immunoarray were accumulated for 15 s with a CCD camera for different analyte concentrations and were processed by subtracting CL intensity from zero cytokine controls ($\sim$10^4 magnitude) to get CL signal intensities (Figure 3). These calibration plots show small standard deviations and linear responses with concentration for each cytokine and CRP. They have linear dynamic ranges of 1 fg/mL to 500 pg/mL for IL-6, 12.5−500 fg/mL for CRP, and 6.25−500 fg/mL for IFN-γ, with an average relative standard deviation of ±8% array to array (n = 5). Limits of detection (LOD) obtained were 0.79 fg/mL for IL-6, 2.7 fg/mL for IFN-γ, and 4.2 fg/mL for CRP. Reproducible CL signal intensity was also obtained for the 3 microwells allotted to each cytokine within a single immunoarray (Figure 3A), giving an average standard deviation of ±6% well to well.

Assay Accuracy Validation. The assay was validated for accuracy in three steps: (i) establishing cross-reactivity between the cytokine antibodies, (ii) measuring spike recoveries of the cytokines in 10-fold diluted pooled human serum (PBS buffer, pH 7.4), and (iii) analyzing patient samples and comparing to mesoscale ELISA-type assays.[76] Sterile, filtered, diluted pooled human serum from healthy subjects was used in the analysis with different concentrations of added cytokines IL-6, IFN-γ, and CRP. The CL signal response was determined in triplicate, and concentrations were obtained after subtracting the relevant signals from the cytokine controls, i.e., diluted pooled human serum. The samples were analyzed using the procedure in Materials and Methods.

We designed assays to check the cross-reactivity between primary and secondary antibodies of each of the cytokines and CRP with the antigens. The assays involved testing one antigen against the Ab$_1$ and Ab$_2$ of the remaining 2 markers under study followed by analysis of the signal obtained as a result of the analysis. From results in Table 1, percent cross-reactivity for the cytokines and CRP lies below 5% in all but 2 cases that

rise to 6−8%. Cross-reactivity measurements were reproducible within ±7%.

Table 1. Cross-Reactivities of Primary and Secondary Antibodies in the 3D-Printed Immunoassay

antigen	percent cross-reactivity with Ab$_1$			percent cross-reactivity with Ab$_2$		
	IL-6 Ab$_1$	CRP Ab$_1$	IFN-γ Ab$_1$	IL-6 Ab$_2$	CRP Ab$_2$	IFN-γ Ab$_2$
IL-6		2.49	2.64		4.65	6.43
CRP	4.36		3.39	8.04		1.84
IFN-γ	2.54	2.30		2.24	1.99	

To confirm the accuracy of the multiplexed 3D-printed immunoassay, spike recoveries of the respective cytokines were measured from spiked pooled human serum samples. Sterile, filtered, 10× PBS-diluted pooled human serum was spiked with different concentrations (15, 60, and 300 fg/mL) of IL-6, CRP, and IFN-γ. This matched dilutions for real cytokine serum assays. Concentrations in spiked samples were found after subtracting the signals for the diluted pooled human serum acting as a control. Calibration curves in pooled human serum were used to estimate recoveries. Recoveries were in the acceptable analytical range for biomedical assays of 100 ± 20%,[77,78] and the average standard deviation was ±6.8% (Table 2). The largest recovery errors of −20% for IL-6 and +17% for IFN-γ were found only at the lowest protein spike concentrations, but they are still within the acceptable range. These results verify the accuracy of the assays and show that the effects of cross-reactivity are negligible.

Patient Sample Analyses. We analyzed 80 COVID-19 patient serum-WHO severity index samples that include 47 mild, 9 moderate, and 24 high severities according to their WHO severity indices. Cytokines IL-6, IFN-γ, and CRP were determined by using the microfluidic array and optimized method. Samples were diluted 10× or 100× in PBS buffer (pH 7.4) for IL-6 and IFN-γ analysis and 100× to 500× for CRP analysis to bring the analyte concentration down into the dynamic range of the assay.

Correlation plots from 3D-printed array assays vs determinations on the same samples using the commercial Meso Scale protein measurement platform (Figure 4) gave a slope of 1.06 and an intercept of 0.47 ± 0.33 pg/mL for IL-6, a slope of 0.89 and an intercept of 8.6 ± 1.90 pg/mL for CRP, and a slope of 0.97 and an intercept of 4.2 ± 0.21 pg/mL for IFN-γ and correlation coefficients (r) close to 1.0. Perfect correlations have a slope and r-value of 1.0 and an intercept of 0.0, so these plots with slopes close to 1.0 and intercepts within 3 standard deviations (SDs) of 0 show a strong positive correlation of the new array results with the established commercial Meso Scale assay for the determination of each of the cytokines and CRP in patient serum.

Diagnostics for Severity. ROC plots were used to estimate the diagnostic specificity and the sensitivity of each of the cytokine levels in patient serum to distinguish different levels of severity indicated by the WHO severity index. Samples were grouped according to low WHO severity scores as a ROC-independent variable zero and high severity WHO score as an independent variable 1 for the ROC plots. Analyzing patient samples grouped into WHO scores 3 and 4 as low severity and WHO scores 7 and 8 as high severity (Figure 5) gave AUC (perfect differentiation = 1, 0) close to

Table 2. Spike Recovery Studies from Multiplexed Immunoassays in Pooled Human Serum ($n = 3$)

spiked concentration (fg/mL)	IL-6		CRP		IFN-γ	
	found concentration	percent recovery	found concentration	percent recovery	found concentration	percent recovery
15.0	12.0	80.0	15.0	99.8	17.5	117.0
60.0	57.5	95.8	58.8	97.9	65.4	109.0
300.0	314.0	105.0	314.0	105.0	288.0	96.0
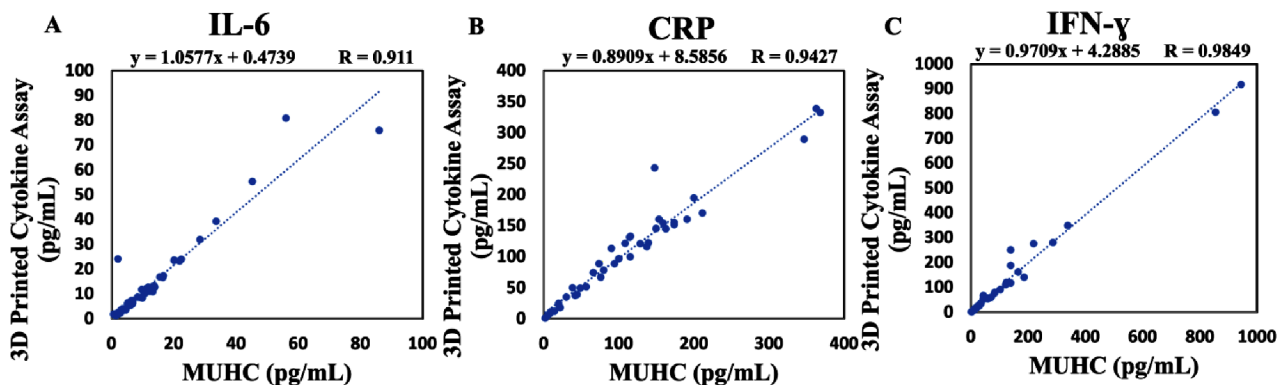
Figure 4. Linear correlation plots for 3D-printed cytokine array vs commercial ELISA-type Meso Scale ECL assay for (A) IL-6, (B) CRP, and (C) IFN-γ, quantified in pg/mL ($n = 3$) in 69 COVID-19 patient samples.
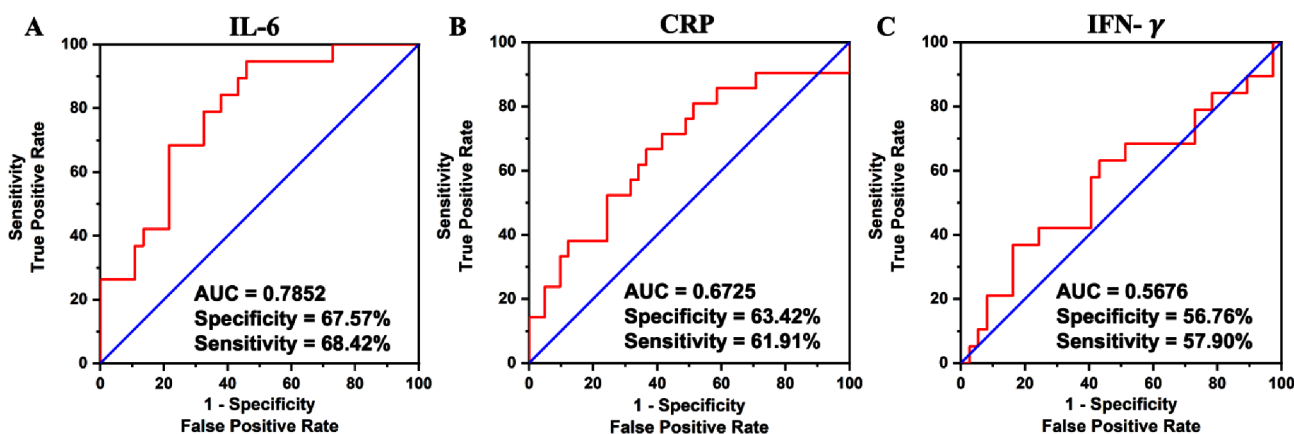
Figure 5. Receiver operating characteristic (ROC) curves for (A) IL-6, (B) CRP, and (C) IFN-γ levels in patient samples comparing low severity (WHO scores 3 and 4) vs high severity (scores 7 and 8). The AUC values obtained are 0.7825, 0.6725, and 0.5676, respectively, under the 95% confidence interval.
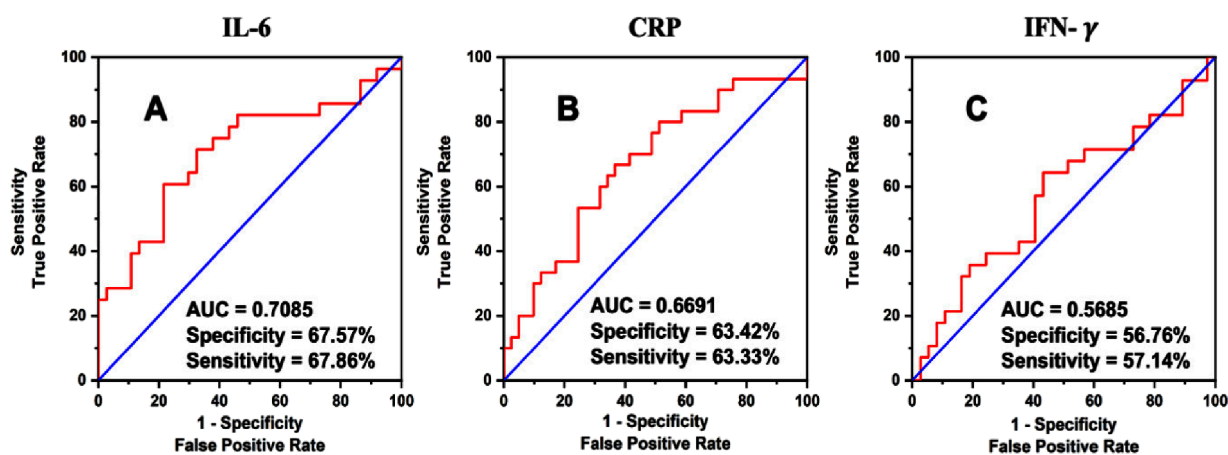
Figure 6. Receiver operating characteristic (ROC) curves for (A) IL-6, (B) CRP, and (C) IFN-γ levels in patient samples comparing low severity (WHO scores 3 and 4) vs moderate severity (scores 5 and 8). The AUC values obtained are 0.7085, 0.6691, and 0.5685, respectively, under the 95% confidence interval.
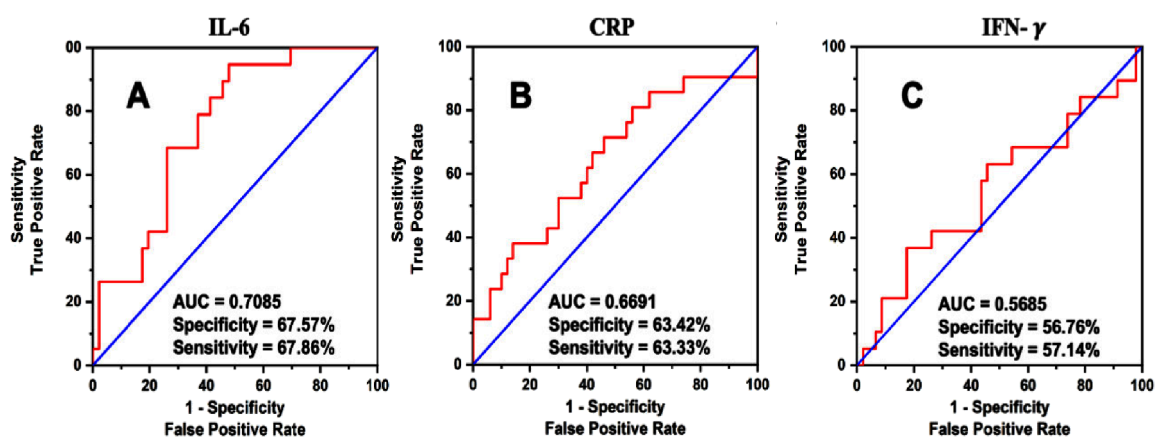
Figure 7. Receiver operating characteristic (ROC) curves for (A) IL-6, (B) CRP, and (C) IFN-γ levels in patient samples comparing low + moderate severity (WHO scores 3 and 6) vs high severity (scores 7 and 8). The AUC values obtained are 0.7825, 0.6725, and 0.5676, respectively, under the 95% confidence interval.

0.7 or above and clinical specificity and sensitivity scores of 62−69% for IL-6 and CPR, showing differentiation of the 2 states (low and high) very well. However, INF-γ shows poorer performance with a ROC AUC of 0.57 and clinical specificity and sensitivity scores <58%. A similar situation pertained for WHO scores 3 and 4 as low severity vs WHO scores 5 and 6 as moderate severity (Figure 6) and WHO scores 3 and 6 combining low and moderate severity vs WHO scores 7 and 8 as high severity (Figure 7), that is, IL-6 and CRP are the good and acceptable biomarkers to differentiate the different classes of severity, while INF-γ is marginal.

DISCUSSION

The immunoarray featuring a unique microwell design in a well-plate format described above facilitates a fast, easy to implement, low-cost, specific, and highly sensitive chemiluminescence assay for the target proteins that takes ~25 min and is suitable for POC single patient assays. The costs are ~$1 per printed array and $2.70 in reagents per assay in the semiautomated 3D-printed microarray. Cytokines can serve as important biomarkers for diseases like COVID-19 where patients can proceed in a matter of hours to a high severity state, and a cytokine increase can signal the onset of a "cytokine storm". In this context, close patient monitoring using a methodology with a rapid turnaround time would have an enormous practical value. In our present study of patient samples, ROC curves of cytokine levels grouped by WHO severity scores comparing low severity (WHO scores 3 and 4) vs high severity (scores 7 and 8) gave the best AUC of 0.78 for IL-6, supporting this biomarker as the best severity indicator among the three pro-inflammatory cytokines measured (Figures 5−7). IL-6 also performed significantly better than CRP, the standard pro-inflammatory cytokine measured routinely to monitor patients affected by COVID-19 upon admission. Further, none of the biomarkers performed very well to distinguish high from moderate severities (Figures 6 and 7) with the highest AUC of 0.71 in these cases, again for IL-6. Although our study was done on a relatively small cohort, our data strongly support the need for rapid availability of IL-6 and possibly CPR measurements in the treatment protocol as critical blood biomarkers for the COVID-19 severity.

The microfluidic immunoassay described detects cytokines with very low LODs, i.e., ~0.79 fg/mL for IL-6, ~4.2 fg/mL for CRP, and ~2.7 fg/mL for IFN-γ.[51] Linear dynamic ranges

of 1−500 fg/mL for IL-6, 12.5−500 fg/mL for CRP, and 6.35−500 fg/mL for IFN-γ were achieved (Figure 3). Samples require dilution in buffer to bring concentration levels into the assay's dynamic range, thus allowing detection of cytokines using volumes of serum samples ≥ 5 μL. These larger dilutions have the added advantage of greatly decreasing concentrations of interferants in the sample, decreasing nonspecific binding, and greatly limiting antibody cross-reactivity. Antibody cross-reactivity in these assays was below 5% in all but 2 cases that were 6−8% (Table 1) in 10-fold diluted pooled human serum, and these values will be much lower in 100- and 500-fold diluted serum than in many of the patient serum assays required. The programmable syringe pump provides semi-automation with precise control in the sequential delivery of reagents to facilitate incubation and washing of the arrays without operator participation.

Accuracy was verified by excellent assay recovery of spiked samples (Table 2), and excellent correlations of the concentrations of each cytokine and CRP from the array to their concentrations were found from commercial Meso Scale assays as seen from the slopes and correlation coefficients close to 1 and intercepts near zero (Figure 4). This rapid, low-cost biomarker assay thus offers great promise for POC use, leading to better management of infection and possible prediction of disease severity and the onset of ARDS.

In summary, we described herein an accurate, ultrasensitive 3D-printed microfluidic immunoarray for POC detection of three cytokines and applied it to serum samples from COVID-19 patients. While we focused on these specific biomarkers, other cytokines previously identified in the context of COVID-19 infection can be easily included or substituted into the array, with additional microwells added as required. The array is suitable for fast, single sample, on-demand POC tests to detect representative cytokines and CRP. IL-6 emerged in this study as the most powerful biomarker for COVID-19 severity. This POC approach is also suitable for serial measurements of cytokines during disease progression as a guide for management. Finally, the array reported here should also be useful for patient care in future coronavirus epidemics.

ASSOCIATED CONTENT

Ⓢ Supporting Information

The Supporting Information is available free of charge at https://pubs.acs.org/doi/10.1021/acsomega.4c00735.

Proteins, chemicals, and supplies; 3D-printed microfluidic immunoarray design and dimensions; concentrations used for the optimization of detection antibodies; optimization of secondary detection antibody Ab_2; concentrations used for the optimization of capture antibodies; optimization of primary capture antibody Ab_1; optimized detection and capture antibodies; estimating the primary antibody coverage in the microwell using bicinchoninic acid assay (BCA); optimization of flow rate using a programmable syringe pump; optimization of incubation time for the complex $Ag-Ab_2-ST-polyHRP$; serum IFN-γ, IL-6, IL-1β, TNF-α, and CRP level in 57 COVID patients; box and whisker plots; receiver operating curve (PDF)

■ AUTHOR INFORMATION

Corresponding Author

James F. Rusling − *Department of Chemistry and Institute of Material Science, University of Connecticut, Storrs, Connecticut 06269, United States; School of Chemistry, National University of Ireland at Galway, Galway H91 TK33, Ireland;* ⊙ orcid.org/0000-0002-6117-3306; Email: james.rusling@uconn.edu

Authors

Ketki S. Bhalerao − *Department of Chemistry, University of Connecticut, Storrs, Connecticut 06269, United States*

P. I. Thilini De Silva − *Department of Chemistry, University of Connecticut, Storrs, Connecticut 06269, United States*

Keshani Hiniduma − *Department of Chemistry, University of Connecticut, Storrs, Connecticut 06269, United States*

Ami Grunbaum − *Department of Medicine, McGill University Health Centre, Montreal, QC H3A 1A1, Canada;* ⊙ orcid.org/0000-0001-8745-0036

Nicholas Rozza − *Department of Medicine, McGill University Health Centre, Montreal, QC H3A 1A1, Canada;* ⊙ orcid.org/0000-0003-1713-8949

Richard Kremer − *Department of Medicine, McGill University Health Centre, Montreal, QC H3A 1A1, Canada*

Complete contact information is available at:
https://pubs.acs.org/10.1021/acsomega.4c00735

Author Contributions

[⊥]K.S.B., P.I.T.D.S., and K.H. contributed equally to this work.

Notes

The authors declare no competing financial interest.
All experiments were performed in accordance with Canadian Guidelines stated in "regulatory framework in health research at the McGill University Health Center" and approved by the ethics committee of the McGill University Health Center. Informed consents were obtained from human participants.

■ REFERENCES

(1) Chakraborty, I.; Maity, P. COVID-19 outbreak: Migration, effects on society, global environment and prevention. *Sci. Total Environ.* **2020**, *728*, 138882−138889.

(2) Di Gennaro, F.; Pizzol, D.; Marotta, C.; Antunes, M.; Racalbuto, V.; Veronese, N.; Smith, L. Coronavirus diseases (COVID-19) current status and future perspectives: a narrative review. *Int. J. Environ. Res. Public Health* **2020**, *17*, 2690−2701.

(3) https://covid19.healthdata.org/global?view=cumulative-deaths&tab=trend (Last accessed on 06/01/2023)

(4) https://www.cdc.gov/coronavirus/2019-ncov/prevent-getting-sick/how-covid-spreads.html (Last accessed on 6/21/2023)

(5) Dramé, M.; Tabue Teguo, M.; Proye, E.; Hequet, F.; Hentzien, M.; Kanagaratnam, L.; Godaert, L. Should RT-PCR be considered a gold standard in the diagnosis of Covid-19. *J. Med. Virol.* **2020**, *92*, 2312−2313.

(6) Brinati, D.; Campagner, A.; Ferrari, D.; Locatelli, M.; Banfi, G.; Cabitza, F. Detection of COVID-19 infection from routine blood exams with machine learning: a feasibility study. *J. Med. Systems* **2020**, *44*, 1−12.

(7) Kanji, J. N.; Zelyas, N.; MacDonald, C.; Pabbaraju, K.; Khan, M. N.; Prasad, A.; Hu, J.; Diggle, M.; Berenger, B. M.; Tipples, G. False negative rate of COVID-19 PCR testing: a discordant testing analysis. *Virol J.* **2021**, *18*, 1−6.

(8) Wang, Y.; Lee, Y.; Yang, T.; Sun, J.; Shen, C.; Cheng, C. Current diagnostic tools for coronaviruses−From laboratory diagnosis to POC diagnosis for COVID-19. *Bioeng. & Trans. Med.* **2020**, *5*, No. e10177.

(9) Lucas, C.; Wong, P.; Klein, J.; Castro, T. B. R.; Silva, J.; Sundaram, M.; Ellingson, M. K.; Mao, T.; Oh, J. E.; Israelow, B.; Takahashi, T.; Tokuyama, M.; Lu, P.; Venkataraman, A.; Park, A.; Mohanty, S.; Wang, H.; Wyllie, A. L.; Vogels, C. B. F.; Earnest, R.; Lapidus, S.; Ott, I. M.; Moore, A. J.; Muenker, M. C.; Fournier, J. B.; Campbell, M.; Odio, C. D.; Casanovas-Massana, A.; Obaid, A.; Lu-Culligan, A.; Nelson, A.; Brito, A.; Nunez, A.; Martin, A.; Watkins, A.; Geng, B.; Kalinich, C.; Harden, C.; Todeasa, C.; Jensen, C.; Kim, D.; McDonald, D.; Shepard, D.; Courchaine, E.; White, E. B.; Song, E.; Silva, E.; Kudo, E.; DeIuliis, G.; Rahming, H.; Park, H. J.; Matos, I.; Nouws, J.; Valdez, J.; Fauver, J.; Lim, J.; Rose, K. A.; Anastasio, K.; Brower, K.; Glick, L.; Sharma, L.; Sewanan, L.; Knaggs, L.; Minasyan, M.; Batsu, M.; Petrone, M.; Kuang, M.; Nakahata, M.; Campbell, M.; Linehan, M.; Askenase, M. H.; Simonov, M.; Smolgovsky, M.; Sonnert, N.; Naushad, N.; Vijayakumar, P.; Martinello, R.; Datta, R.; Handoko, R.; Bermejo, S.; Prophet, S.; Bickerton, S.; Velazquez, S.; Alpert, T.; Rice, T.; Khoury-Hanold, W.; Peng, X.; Yang, Y.; Cao, Y.; Strong, Y.; Herbst, R.; Shaw, A. C.; Medzhitov, R.; Schulz, W. L.; Grubaugh, N. D.; Dela Cruz, C.; Farhadian, S.; Ko, A. I.; Omer, S. B.; Iwasaki, A. Longitudinal analyses reveal immunological misfiring in severe COVID-19. *Nature* **2020**, *584*, 463−469.

(10) Ni, L.; Ye, F.; Cheng, M. L.; Feng, Y.; Deng, Y. Q.; Zhao, H.; Wei, P.; Ge, J.; Gou, M.; Li, X.; Sun, L.; Cao, T.; Wang, P.; Zhou, C.; Zhang, R.; Liang, P.; Guo, H.; Wang, X.; Qin, C.; Chen, F.; Dong, C. Detection of SARS-CoV-2-specific humoral and cellular immunity in COVID-19 convalescent individuals. *Immunity* **2020**, *52*, 971−977.

(11) Subbarao, K.; Mahanty, S. Respiratory virus infections: understanding COVID-19. *Immunity* **2020**, *52*, 905−909.

(12) Tay, M. Z.; Poh, C. M.; Rénia, L.; MacAry, P. A.; Ng, L. F. The trinity of COVID-19: immunity, inflammation and intervention. *Nat. Rev.s. Immunol.* **2020**, *20*, 363−374.

(13) Maranini, B.; Ciancio, G.; Ferracin, M.; Cultrera, R.; Negrini, M.; Sabbioni, S.; Govoni, M. microRNAs and inflammatory immune response in SARS-CoV-2 infection: a narrative review. *Life* **2022**, *12* (2), 288−305.

(14) Guo, J.; Wang, S.; Xia, H.; Shi, D.; Chen, Y.; Zheng, S.; Chen, Y.; Gao, H.; Guo, F.; Ji, Z.; Huang, C.; Luo, R.; Zhang, Y.; Zuo, J.; Chen, Y.; Xu, Y.; Xia, J.; Zhu, C.; Xu, X.; Qiu, Y.; Sheng, J.; Xu, K.; Li, L. Cytokine signature associated with disease severity in COVID-19. *Front. in Immunol.* **2021**, *12*, 681516−681526.

(15) Mittal, R.; Chourasia, N.; Bharti, V. K.; Singh, S.; Sarkar, P.; Agrawal, A.; Ghosh, A.; Pal, R.; Kanwar, J.; Kotnis, A. Blood-based

biomarkers for diagnosis, prognosis, and severity prediction of COVID-19: Opportunities and challenges. *J. of Family Med. and Pri. Care* **2022**, *11*, 4330−4341.

(16) Gallo Marin, B.; Aghagoli, G.; Lavine, K.; Yang, L.; Siff, E. J.; Chiang, S. S.; Salazar- Mather, T. P.; Dumenco, L.; Savaria, M. C.; Aung, S. N.; Flanigan, T.; Michelow, I. C. Predictors of COVID-19 severity: a literature review. *Rev. in Med.l. virol.* **2021**, *31*, 1−10.

(17) Monastero, R. N.; Pentyala, S. Cytokines as biomarkers and their respective clinical cutoff levels. *Int. J. of inflammation* **2017**, *2017*, 1−11.

(18) Hopkins, S. J. The pathophysiological role of cytokines. *Legal Med.* **2003**, *5*, S45−S57.

(19) Corwin, E. J. Understanding cytokines part I: physiology and mechanism of action. *Bio.l research for nursing* **2000**, *2*, 30−40.

(20) Arango Duque, G.; Descoteaux, A. Macrophage cytokines: involvement in immunity and infectious diseases. *Front. in Immunol.* **2014**, *5*, 491−503.

(21) https://en.wikipedia.org/wiki/Cytokine_storm (Last accessed on 06/21/2023)

(22) Fajgenbaum, D. C.; June, C. H. Cytokine storm. *New England J. of Med.* **2020**, *383*, 2255−2273.

(23) Braciale, T. J.; Hahn, Y. S. Immunity to viruses. *Immuno.l. reviews* **2013**, *255*, 5−12.

(24) Shimizu, M. Clinical features of cytokine storm syndrome. *Cytokine storm syndrome* **2019**, 31−41.

(25) Coperchini, F.; Chiovato, L.; Ricci, G.; Croce, L.; Magri, F.; Rotondi, M. The cytokine storm in COVID-19: Further advances in our understanding the role of specific chemokines involved. *Cytokine & Growth Factor Rev.* **2021**, *58*, 82−91.

(26) Burke, H.; Freeman, A.; Cellura, D. C.; Stuart, B. L.; Brendish, N. J.; Poole, S.; Borca, F.; Phan, H. T. T.; Sheard, N.; Williams, S.; Spalluto, C. M.; Staples, K. J.; Clark, T. W.; Wilkinson, T. M. A.; Wilkinson, T.; Freeman, A.; Burke, H.; Dushianthan, A.; Celinski, M.; Batchelor, J.; Faust, S. N.; Thomas, G.; Kipps, C. REACT COVID investigators Tom Wilkinson Anna Freeman Hannah Burke Ahilanadan Dushianthan Michael Celinski James Batchelor Saul N. Faust Gareth Thomas Christopher Kipps. Inflammatory phenotyping predicts clinical outcome in COVID-19. *Respir. Res.* **2020**, *21*, 245.

(27) Herold, T.; Jurinovic, V.; Arnreich, C.; Lipworth, B. J.; Hellmuth, J. C.; von Bergwelt-Baildon, M.; Klein, M.; Weinberger, T. Elevated levels of IL-6 and CRP predict the need for mechanical ventilation in COVID-19. *J. Aller. Clin.l Immunol.* **2020**, *146*, 128−136.

(28) Huang, C.; Wang, Y.; Li, X.; Ren, L.; Zhao, J.; Hu, Y.; Zhang, L.; Fan, G.; Xu, J.; Gu, X.; Cheng, Z.; Yu, T.; Xia, J.; Wei, Y.; Wu, W.; Xie, X.; Yin, W.; Li, H.; Liu, M.; Xiao, Y.; Gao, H.; Guo, L.; Xie, J.; Wang, G.; Jiang, R.; Gao, Z.; Jin, Q.; Wang, J.; Cao, B. Clinical features of patients infected with 2019 novel coronavirus in Wuhan, China. *Lancet* **2020**, *395*, 497−506.

(29) Li, H.; Liu, L.; Zhang, D.; Xu, J.; Dai, H.; Tang, N.; Su, X.; Cao, B. SARS-CoV-2 and viral sepsis: observations and hypotheses. *Lancet* **2020**, *395*, 1517−1520.

(30) Huang, Q.; Wu, X.; Zheng, X.; Luo, S.; Xu, S.; Weng, J. Targeting inflammation and cytokine storm in −19. *Pharmacol.l Res.* **2020**, *159*, 105051−105054.

(31) Han, H.; Ma, Q.; Li, C.; Liu, R.; Zhao, L.; Wang, W.; Zhang, P.; Liu, X.; Gao, G.; Liu, F.; Jiang, Y.; Cheng, X.; Zhu, C.; Xia, Y. Profiling serum cytokines in COVID-19 patients reveals IL-6 and IL-10 are disease severity predictors. *Emerg. microbes & infect.* **2020**, *9*, 1123−1130.

(32) Melo, A. K. G.; Milby, K. M.; Caparroz, A. L. M. A.; Pinto, A. C. P. N.; Santos, R. R. P.; Rocha, A. P.; Ferreira, G. A.; Souza, V. A.; Valadares, L. D. A.; Vieira, R. M. R. A.; Pileggi, G. S.; Trevisani, V. F. M.; Chalmers, J. Biomarkers of cytokine storm as red flags for severe and fatal COVID-19 cases: A living systematic review and meta-analysis. *PloS one* **2021**, *16*, e0253894.

(33) Mehta, P.; McAuley, D. F.; Brown, M.; Sanchez, E.; Tattersall, R. S.; Manson, J. J. COVID-19: consider cytokine storm syndromes and immunosuppression. *lancet* **2020**, *395*, 1033−1034.

(34) Schulert, G. S.; Grom, A. A. Pathogenesis of macrophage activation syndrome and potential for cytokine-directed therapies. *Annu. Rev. of Med.* **2015**, *66*, 145−159.

(35) Wang, L. C-reactive protein levels in the early stage of COVID-19. *Med. et maladies infectieuses* **2020**, *50*, 332−334.

(36) Ruan, Q.; Yang, K.; Wang, W.; Jiang, L.; Song, J. Clinical predictors of mortality due to COVID-19 based on an analysis of data of 150 patients from Wuhan, China. *Intensive care Med.* **2020**, *46*, 846−848.

(37) Zhou, F.; Yu, T.; Du, R.; Fan, G.; Liu, Y.; Liu, Z.; Xiang, J.; Wang, Y.; Song, B.; Gu, X.; Guan, L.; Wei, Y.; Li, H.; Wu, X.; Xu, J.; Tu, S.; Zhang, Y.; Chen, H.; Cao, B. Clinical course and risk factors for mortality of adult inpatients with COVID-19 in Wuhan, China: a retrospective cohort study. *lancet* **2020**, *395*, 1054−1062.

(38) Wang, D.; Hu, B.; Hu, C.; Zhu, F.; Liu, X.; Zhang, J.; Wang, B.; Xiang, H.; Cheng, Z.; Xiong, Y.; Zhao, Y.; Li, Y.; Wang, X.; Peng, Z. Clinical characteristics of 138 hospitalized patients with 2019 novel coronavirus−infected pneumonia in Wuhan. *China. jama* **2020**, *323*, 1061−1069.

(39) Liu, G.; Jiang, C.; Lin, X.; Yang, Y. Point-of-care detection of cytokines in cytokine storm management and beyond: Significance and challenges. *View* **2021**, *2*, 20210003−202110022.

(40) Mathers, A. J. The practical challenges of making clinical use of the quantitative value for SARS-CoV-2 viral load across several dynamics. *Clin. Infect. Dis.* **2021**, *73* (11), No. e4206.

(41) Magleby, R.; Westblade, L. F.; Trzebucki, A.; Simon, M. S.; Rajan, M.; Park, J.; Goyal, P.; Safford, M. M.; Satlin, M. J. Impact of Severe Acute Respiratory Syndrome Coronavirus 2 Viral Load on Risk of Intubation and Mortality Among Hospitalized Patients With Coronavirus Disease 2019. *Clin. Infect. Dis.* **2021**, *73*, No. e4197.

(42) Shah, S.; Singhal, T.; Davar, N.; Thakkar, P. No correlation between Ct values and severity of disease or mortality in patients with COVID 19 disease. *Indian J. Med. Microbiol.* **2021**, *39*, 116−117.

(43) Ong, D. S. Y.; Fragkou, P. C.; Schweitzer, V. A.; Chemaly, R. F.; Moschopoulos, C. D.; Skevaki, C. How to interpret and use COVID-19 serology and immunology tests. *Clin Microbiol Infect.* **2021**, *27*, 981−986.

(44) Aziz, N. Measurement of circulating cytokines and immune-activation markers by multiplex technology in the clinical setting: what are we really measuring? *Onco Therapeutics* **2015**, *6* (1−2), 19−22.

(45) Shankar, G.; Cohen, D. A. Enhanced cytokine detection by a novel cell culture-based ELISA. *J. of Immunoass. and Immunochem.* **1997**, *18* (4), 371−388.

(46) https://www.rndsystems.com/products/luminex-assays-and-high-performance-assays (Last accessed on 03/13/2024)

(47) https://www.quanterix.com/instruments/simoa-hd-x-analyzer/ (Last accessed on 03/13/2024)

(48) Rissin, D. M.; Kan, C. W.; Campbell, T. G.; Howes, S. C.; Fournier, D. R.; Song, L.; Piech, T.; Patel, P. P.; Chang, L.; Rivnak, A.; Ferrell, E. P.; Randall, J. D.; Provuncher, G. K.; Walt, D. R.; Duffy, D. C. Single-molecule enzyme-linked immunosorbent assay detects serum proteins at subfemtomolar concentrations. *Nat. Biotechnol.* **2010**, *28* (6), 595−599. **2010**

(49) Song, Y.; Ye, Y.; Su, S. H.; Stephens, A.; Cai, T.; Chung, M. T.; Han, M. K.; Newstead, M. W.; Yessayan, L.; Frame, D.; Humes, H. D.; Singer, B. H.; Kurabayashi, K. A digital protein microarray for COVID-19 cytokine storm monitoring. *Lab Chip* **2021**, *21* (2), 331−343.

(50) Wilson, D. H.; Rissin, D. M.; Kan, C. W.; Fournier, D. R.; Piech, T.; Campbell, T. G.; Meyer, R. E.; Fishburn, M. W.; Cabrera, C.; Patel, P. P.; Frew, E.; Chen, Y.; Chang, L.; Ferrell, E. P.; von Einem, V.; McGuigan, W.; Reinhardt, M.; Sayer, H.; Vielsack, C.; Duffy, D. C. The Simoa HD-1 analyzer: a novel fully automated digital immunoassay analyzer with single-molecule sensitivity and multiplexing. *J. of Lan. Autom.* **2016**, *21* (4), 533−547.

(51) Vásquez, V.; Orozco, J. Detection of COVID-19-related biomarkers by electrochemical biosensors and potential for diagnosis,

prognosis, and prediction of the course of the disease in the context of personalized medicine. *Anal. Bioanal.l Chem.* **2023**, *415*, 1003−1031.

(52) Tan, C.; Huang, Y.; Shi, F.; Tan, K.; Ma, Q.; Chen, Y.; Jiang, X.; Li, X. C-reactive protein correlates with computed tomographic findings and predicts severe COVID-19 early. *J. Med. Virol.* **2020**, *92*, 856−862.

(53) Liu, F.; Li, L.; Xu, M.; Wu, J.; Luo, D.; Zhu, Y.; Li, B.; Song, X.; Zhou, X. Prognostic value of interleukin-6, C-reactive protein, and procalcitonin in patients with COVID-19. *J. Clin. Virol.* **2020**, *127*, 104370−104375.

(54) Xu, Z. S.; Shu, T.; Kang, L.; Wu, D.; Zhou, X.; Liao, B. W.; Sun, X. L.; Zhou, X.; Wang, Y. Y. Temporal profiling of plasma cytokines, chemokines, and growth factors from mild, severe and fatal COVID-19 patients. *Signal trans. Targeted Ther.* **2020**, *5*, 100−103.

(55) Del Valle, D. M.; Kim-Schulze, S.; Huang, H. H.; Beckmann, N. D.; Nirenberg, S.; Wang, B.; Lavin, Y.; Swartz, T. H.; Madduri, D.; Stock, A.; Marron, T. U.; Xie, H.; Patel, M.; Tuballes, K.; Van Oekelen, O.; Rahman, A.; Kovatch, P.; Aberg, J. A.; Schadt, E.; Jagannath, S.; Mazumdar, M.; Charney, A. W.; Firpo-Betancourt, A.; Mendu, D. R.; Jhang, J.; Reich, D.; Sigel, K.; Cordon-Cardo, C.; Feldmann, M.; Parekh, S.; Merad, M.; Gnjatic, S. An inflammatory cytokine signature helps predict COVID-19 severity and death. *medRxiv* **2020**, *26*, 1636−1643.

(56) Buszko, M.; Nita-Lazar, A.; Park, J. H.; Schwartzberg, P. L.; Verthelyi, D.; Young, H. A.; Rosenberg, A. S. Lessons learned: new insights on the role of cytokines in COVID-19. *Na. Immuno.* **2021**, *22*, 404−411.

(57) Akhmerov, A.; Marbán, E. COVID-19 and the heart. *Circ. Res.* **2020**, *126*, 1443−1455.

(58) Huespe, I.; Carboni Bisso, I.; Di Stefano, S.; Terrasa, S.; Gemelli, N. A.; Las Heras, M. COVID-19 Severity Index: A predictive score for hospitalized patients. *Med. Intensiva.* **2022**, *46*, 98−101.

(59) Hiniduma, K.; Bhalerao, K. S.; De Silva, P. I. T.; Chen, T.; Rusling, J. F. Design and Fabrication of a 3D-Printed Microfluidic Immunoarray for Ultrasensitive Multiplexed Protein Detection. *Micromachines* **2023**, *14*, 2187−2206.

(60) Chauhan, N.; Saxena, K.; Jain, U. Single molecule detection; from microscopy to sensors. *Int. J. Biol. Macromolecules* **2022**, *209*, 1389−1401.

(61) Liu, G.; Jiang, C.; Lin, X.; Yang, Y.; Point-of-care detection of cytokines in cytokine storm management and beyond: Significance and challenges, *VIEW.* **2021**, 2:20210003, / DOI: .

(62) Ding, S.; Mosher, C.; Lee, X. Y.; Das, S. R.; Cargill, A. A.; Tang, X.; Chen, B.; McLamore, E. S.; Gomes, C.; Hostetter, J. M.; Claussen, J. C. Rapid and label-free detection of interferon gamma via an electrochemical aptasensor comprising a ternary surface monolayer on a gold interdigitated electrode array. *Acs Sensors* **2017**, *2* (2), 210−217.

(63) Sharafeldin, M.; Kadimisetty, K.; Bhalerao, K. S.; Chen, T.; Rusling, J. F. 3D-printed Immunosensor arrays for cancer diagnostics. *Sensors* **2020**, *20*, 4514.

(64) Parate, K.; Rangnekar, S. V.; Jing, D.; Mendivelso-Perez, D. L.; Ding, S.; Secor, E. B.; Smith, E. A.; Hostetter, J. M.; Hersam, M. C.; Claussen, J. C. Aerosol-jet-printed graphene immunosensor for label-free cytokine monitoring in serum. *ACS Appl. Mater. Interfaces* **2020**, *12*, 8592−8603.

(65) Sánchez-Tirado, E.; Salvo, C.; González-Cortés, A.; Yáñez-Sedeño, P.; Langa, F.; Pingarrón, J. M. Electrochemical immuno-sensor for simultaneous determination of interleukin-1 beta and tumor necrosis factor alpha in serum and saliva using dual screen printed electrodes modified with functionalized double−walled carbon nanotubes. *Analytica chimica acta* **2017**, *959*, 66−73.

(66) Sharafeldin, M.; Kadimisetty, K.; Bhalerao, K. R.; Bist, I.; Jones, A.; Chen, T.; Lee, N. H.; Rusling, J. F. Accessible telemedicine diagnostics with ELISA in a 3D printed pipette tip. *Anal. Chem.* **2019**, *91*, 7394−7402.

(67) Sharafeldin, M.; Chen, T.; Ozkaya, G. U.; Choudhary, D.; Molinolo, A. A.; Gutkind, J. S.; Rusling, J. F. Detecting cancer metastasis and accompanying protein biomarkers at single cell levels

using a 3D-printed microfluidic immunoarray. *Biosens. and Bioelectron.* **2021**, *171*, 112681−112691.

(68) Smith, P. E.; Krohn, R. I.; Hermanson, G. T.; Mallia, A. K.; Gartner, F. H.; Provenzano, M.; Fujimoto, E. K.; Goeke, N. M.; Olson, B. J.; Klenk, D. C. Measurement of protein using bicinchoninic acid. *Anal. Biochem.* **1985**, *150*, 76−85.

(69) Feng, M.; Berdugo Morales, A.; Poot, A.; Beugeling, T.; Bantjes, A. Effects of Tween 20 on the desorption of proteins from polymer surfaces. *J. of Biomats. Sci., Polymer Edition* **1996**, *7* (5), 415−424. **1996**

(70) Zhang, W.; Ang, W. T.; Xue, C. Y.; Yang, K. L. Minimizing nonspecific protein adsorption in liquid crystal immunoassays by using surfactants. *ACS Appl. Mater. Interfaces* **2011**, *3* (9), 3496−3500.

(71) Kenny, G. E.; Dunsmoor, C. L. Effectiveness of detergents in blocking nonspecific binding of IgG in the enzyme-linked immunosorbent assay (ELISA) depends upon the type of polystyrene used. *Isr. J.l of Med. Sci.* **1987**, *23* (6), 732−734.

(72) Chi, Y. S.; Byon, H. R.; Choi, H. C.; Choi, I. S. A Noncovalent Approach to the Construction of Tween 20-Based Protein Micro-arrays. *ChemBioChem.* **2007**, *8* (12), 1380−1387.

(73) Rubio-Rivas, M.; Mora-Luján, J. M.; Formiga, F.; Arévalo-Cañas, C.; Lebrón Ramos, J. M.; Villalba García, M. V.; Fonseca Aizpuru, E. M.; Díez-Manglano, J.; Arnalich Fernández, F.; Romero Cabrera, J. L.; García García, G. M.; Pesqueira Fontan, P. M.; Vargas Núñez, J. A.; Freire Castro, S. J.; Loureiro Amigo, J.; Pascual Pérez, M. d. l. R.; Alcalá Pedrajas, J. N.; Encinas-Sánchez, D.; Mella Pérez, C.; Ena, J.; Gracia Gutiérrez, A.; Esteban Giner, M. J.; Varona, J. F.; Millán Núñez-Cortés, J.; Casas-Rojo, J. M. WHO Ordinal Scale and Inflamation Risk in COVID-19. *J. Gen. Int. Med.* **2022**, *37*, 1980−1987.

(74) Zweig, M. H.; Campbell, G. Receiver-operating characteristic (ROC) plots. *Clin. Chem.* **1993**, *39*, 561−577.

(75) ROC software: https://www.medcalc.org/download.php and https://www.medcalc.org/features/roccurves.php (Last accessed/downloaded 02/19/2020)

(76) Yu, X.; Munge, B.; Patel, V.; Jensen, G.; Bhirde, A.; Gong, J. D.; Kim, S. N.; Gillespie, J.; Gutkind, S.; Papadimitrakopoulos, F.; Rusling, J. F. Carbon Nanotube Amplification Strategies for Highly Sensitive Immunosensing of Cancer Biomarkers in Serum and Tissue. *J. Am. Chem. Soc.* **2006**, *128*, 11199−11205.

(77) Shah, V. P.; Midha, K. K.; Findlay, J. W. A.; Hill, H. M.; Hulse, J. D.; McGilveray, I. J.; McKay, G.; Miller, K. J.; Patnaik, R. N.; Powell, M. L.; Tonelli, A.; Viswanathan, C. T.; Yacobi, A. Bioanalytical method validation—a revisit with a decade of progress. *Pharm. Res.* **2000**, *17*, 1551−1557.

(78) Harris, D. C. *Quantitative chemical analysis*; Macmillan, W.H. Freeman and company: New York, 2010; pp- 70- 90.